Research on Chemical Intermediates (2019) 45:4163–4177
https://doi.org/10.1007/s11164-019-03898-x

UV–Vis spectroscopy and desorption/ionization mass spectrometry as the tools for investigation of adsorbed dye photodegradation

N. Smirnova[1] · A. Eremenko[1] · T. Fesenko[1] · M. Kosevich[2] · S. Snegir[1]

Received: 22 January 2019 / Accepted: 9 April 2019 / Published online: 19 June 2019

Abstract

The photodegradation of the cationic dyes methylene blue, acridine yellow and acridine orange adsorbed on TiO_2, TiO_2/SiO_2, SiO_2 and Ag/SiO_2 mesoporous films has been studied by electronic spectroscopy and laser desorption/ionization mass-spectrometry methods. Qualitative difference of peak intensity distribution for cation M^+ and its reduced forms $[M+H]^{+\cdot}$ and $[M+2H]^+$ has been detected in the laser desorption/ionization mass spectra of the dye adsorbed on the three film types. The results point out the sensitivity of the laser desorption/ionization mass spectra parameters to specific features of the dye cation adsorption on films of different compositions and photocatalytic activity. Characteristic dependencies of mass spectra intensities upon the duration of UV irradiation have been obtained for dyes adsorbed on the catalytically active films. Some products of the dye photodestruction have been identified, and it has been shown that photo-catalytic activity decreased in the order $TiO_2 > SiO_2/TiO_2 > SiO_2$. In the presence of titania, photobleaching of adsorbed dyes occurs faster in comparison with this process in the presence of SiO_2 and leads to the full discoloration and degradation of adsorbed dye molecules. Efficient photodegradation of acridine dyes occurs through the following steps: 1-N-demethylation (deamination for AY); 2-photodimerization; 3-photodegradation. It is shown that both the rise of Ag nanoparticle concentration on the surface of mesoporous silica films and the enlargement of the nanoparticles' size from 3 to 6–12 nm intensified methylene blue desorption/ionization. The efficiency of mesoporous nanosized TiO_2, SiO_2/TiO_2, SiO_2 and Ag/SiO_2 films as substrates for laser desorption/ionization mass-spectrometry method has been demonstrated.

Keywords Mesoporous TiO_2 · SiO_2 · Ag/SiO_2 · Photodegradation of dyes · UV–Vis spectroscopy · LDI mass-spectrometry

✉ N. Smirnova
smirnatali@gmail.com

Extended author information available on the last page of the article

Introduction

Mesoporous homogeneous transparent oxide films based on TiO_2 and SiO_2 were prepared via template sol–gel method. Noble metal nanoparticles (NPs) on their surface dramatically increase the photocatalytic activity of such oxides in ecologically important processes of destruction of organic and inorganic toxic compounds (industrial dyes, heavy metals ions, pesticides). Organic dyes such as acridine, xanthene and thiazine derivatives are considered in the search for photosensitizers in energy projects [1–7], in the development of water and air purification systems, self-cleaning surfaces, and polymers. Photoinduced transfer of an electron and a proton underlie such processes. Modification of the films by nanoparticles of noble metals enhances their photocatalytic activity by 30–50% due to more efficient charge separation in the bandgap of a photocatalyst. We have developed methods of production and modification of new composite film materials (binary oxides SiO_2/TiO_2, SiO_2/ZrO_2, etc.) with controlled porosity and high photocatalytic activity, including films activated by Ag and Au NPs [8–10].

A large number of publications on dye photodegradation using TiO_2-containing catalysts are devoted to the estimation of the photocatalysts' efficiency. Monitoring of photodegradation has been performed using liquid chromatography or by spectral methods assessing the degree of bleaching [11], transformations of UV or IR spectra [12], and decreasing total organic carbon [7, 13–15]. The photobleaching of methylene blue (MB) via its colorless leuco form as the first stage of the photocatalytic process in the presence of TiO_2 in an aqueous solution was reported in [16]. The application of the abovementioned methods is limited by their insufficiently low sensitivity and the inability to identify reaction intermediates (often more toxic than the original pollutant) due to their short lifetime and low concentration. The use of mass spectrometry in laser desorption/ionization (LDI) mode with simultaneous spectral studies of dyes adsorbed on transparent films in a wide spectral range of mesoporous films allows us to solve these problems [17, 18]. For example, the matrix-assisted LDI (MALDI) mass spectrometry experiments allowed identification of the mechanism of photocatalytic degradation of tetracycline hydrochloride via gold-containing zinc-titanium oxide films [19].

The produced mesoporous films appeared to be promising substrates for studies of electron and proton transfer processes and excitation energy migration between an inorganic matrix and adsorbed molecules by LDI mass-spectrometry (LDI-MS) method. In previous works, we investigated the influence of the nature of the surface on the photodegradation and the mechanism of photocatalytic decomposition of MB with mass spectrometric identification of intermediates [16, 20, 21]. The conditions of the LDI experiment were optimized in [22], and the possibility of in situ analysis of the dye photobleaching and their aggregation was shown.

The combination of theoretical modelling, electronic spectroscopy and LDI-MS methods facilitates obtaining reliable data on the mechanisms and kinetics of adsorbed dye molecule destruction under UV irradiation on the surface of

photocatalytically active mesoporous films and identification of dye photodegradation intermediates [23]. The effect of treatment temperature on photocatalytic activity of TiO_2 films and the mechanism of stearic acid photodegradation has been studied via combination of FT-IR and LDI spectroscopy [24]. The great potential of these films for applications in LDI spectroscopy as substrates (wafers) with variable hydrophilic properties was shown. Influence of size-selected Ag nanoparticles in mesoporous silica films onto reinforcement of ion yield under conditions of LDI was discussed [25].

This work is devoted to the investigation of photoinduced processes on the surface of titania- and silica-based nanomaterials. The correlation between spectroscopic and mass spectrometry data as well as an increase in the sensitivity of LDI-MS experiment using the surface-enhancing phenomena are discussed.

Experimental

The template sol–gel method was applied for preparation of thin optically transparent films of titanium dioxide, titania-silica and silica with developed porosity on glass substrate [8–10]. To obtain a precursor of TiO_2 and SiO_2 films, acid hydrolysis of titanium tetraisopropoxide (TIPT) or tetraethoxysilane (TEOS) was carried out in the presence of triblock copolymer polyethylene oxide/polypropylene oxide Pluronix P123 as the template. To obtain the TiO_2/SiO_2 films, TIPT was mixed with pre-hydrolyzed water/ethanol solution of TEOS. 1 M HNO_3 solution was used to adjust the pH value on hydrolysis of TEOS. To form Ag NPs within the oxide films, $AgNO_3$ was added to the precursor sols. The concentration of Ag^+ ions was varied from 3 to 10 at%. For film deposition onto glass substrates, a dip-coating technique was applied. The pore structure of films defines uniform size distribution of Ag NPs [9]. The specific surface area of the films is 600–700 m^2/g with average pore size of 8–20 nm. In accordance with XRD measurements, titania-based films consist of anatase nanoparticles with the average size of 10–15 nm [9]. Freshly prepared SiO_2 and TiO_2/SiO_2 films showed highly hydrophilic properties, (water contact angles being ca. 10–20°). TiO_2 films after calcination at 350 °C show a contact angle near 32°. After UV illumination (10 min in air under mercury lamp light), the mesoporous TiO_2 films exhibited photoinduced super-hydrophilicity with a water contact angle near 0° [24].

Optical spectra (transmission mode) of the films were recorded using a Lambda UV–Vis spectrometer (Perkin Elmer).

Dyes were adsorbed on the surface of films from the aqueous solution. Adsorption was controlled by electronic spectra. The adsorption isotherms of methylene blue (MB), acridine yellow (AY) and acridine orange (AO) showed a Langmuir character, indicating monomolecular adsorption. The photoinduced destruction of adsorbed dyes was performed by irradiating with a PRK-1000 mercury lamp with $\lambda = 254$ nm and a light density of 1017 quanta cm^{-2}. To study the dynamics of the process, the absorption spectra and the dye mass spectra with the LDI method were recorded.

Laser desorption/ionization time-of-flight mass spectrometry was carried out in positive-ion extraction mode on a Bruker Daltonics Autoflex II instrument (3-ns pulse laser fluency 60 mj/cm^2; accelerating voltage 20 keV; nitrogen UV laser at 337-nm wavelength; linear detection mode, delayed extraction 10 ns). Data averaging by means of spectra summation on the different spots of the substrate surface under fixed instrument parameters was provided for acquisition of the resulting mass spectra.

Results and discussion

Studies of photoinduced charge transfer (PET) elementary oxidation/reduction reactions and molecular association of adsorbed dyes are widely investigated for acridine dyes and MB [2, 6, 26, 27]. Mesoporous TiO_2 and SiO_2 films were successfully used as substrates for mass spectrometry analysis of dyes using laser desorption/ionization (LDI) [20], since LDI mass spectra of dyes deposited on TiO_2, SiO_2 and TiO_2/SiO_2 contain intensive signals with minimal fragmentation of dye. Due to their transparency, the mesoporous TiO_2, SiO_2/TiO_2 and SiO_2 films being active substrates made it possible to investigate photocatalytic processes in situ, simultaneously recording changes in the absorption spectra and mass spectra of the adsorbed dye.

UV–Vis and LDI mass spectra of cationic dyes adsorbed on TiO_2, SiO_2 and TiO_2/SiO_2

The spectra of MB adsorbed on the surface of mesoporous SiO_2 and TiO_2/SiO_2 films (Fig. 1) show an increase in the intensity of the dimeric form ($\lambda = 614$ nm) of MB relative to the monomeric one ($\lambda = 660$ nm) in comparison with the same in the solution [28]. The formation of the dimeric form of adsorbed MB occurred within pores also. In the MB spectrum on TiO_2, the effect of metachromasy was observed [12, 29] with a hypsochromic shift of the absorption maximum from 614 to 570 nm

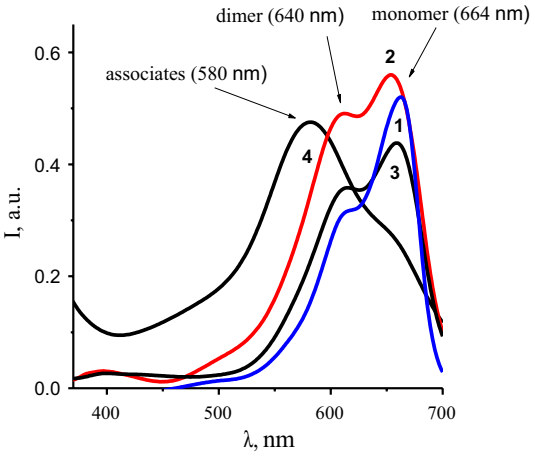

Fig. 1 Absorption spectra of MB in water solution (1); MB adsorbed on the film surfaces: SiO_2 (2); TiO_2/SiO_2 (3) and TiO_2 (4)

(Fig. 1, 4). A strong metachromatic effect observed for the basic blue dye adsorbed on TiO_2 films has been signed [30] to the dye molecules' aggregation onto a hydrophilic film surface.

In LDI spectra of MB adsorbed on TiO_2 films, the peaks corresponding to dimers and the semi-reduced form of MB indicate they are practically suppressed on SiO_2 films [20]. Charge transfer reactions proceed more actively in the "dye-TiO_2" systems than in the "dye-SiO_2" system. The qualitative differences in the distribution of the intensity of the peaks of MB cation (C16H18N3S), (M^+) and its reduced forms ($[M+H]^{\cdot+}$, $[M+2\,H]^+$), in the mass spectra of the adsorbed dye are shown (Fig. 2). It has been found that the reduced forms of MB are practically absent using the standard (metal) target and substrate SiO_2.

The most effective reduction is achieved on the TiO_2 substrates. This is manifested in mass spectra by domination of the ion peak which is the result of a one-electron reduction $[M^+ + e^- + H^+ \rightarrow (M+H)^{+\cdot}]$, and the significant intensity of the peak corresponds to the product of the two-electron reduction $[M^+ + 2e^- + H^+ \rightarrow (M+H)^o]$—the leuco form of MB—which is neutral, and it can only be observed in mass spectra as the protonated form $[M+2H]^+$.

In LDI spectra of MB on TiO_2 substrate, some peaks of dimer double-charged ions are observed. These results correlate with the electronic spectra, according to which TiO_2 coatings contribute to the formation of dimer forms at adsorption (Fig. 1, curve 4).

The absorption spectra of acridine dyes (Fig. 3) differ significantly depending on the film composition. According to the electron absorption spectra, AO is adsorbed on oxide films predominantly in the form of dimers stabilized by the stacking interaction of the aromatic systems of its molecules. This is evidenced

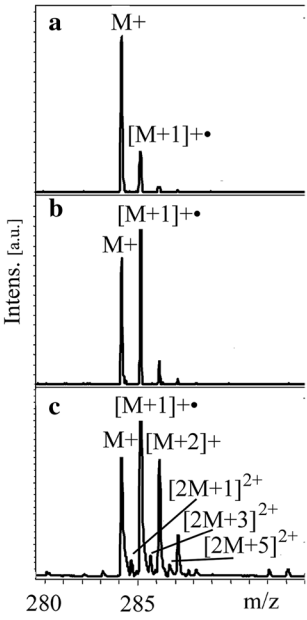

Fig. 2 Fragments of LDI mass spectra of MB adsorbed on SiO_2 (**a**) TiO_2/SiO_2 (**b**) and TiO_2 (**c**) films

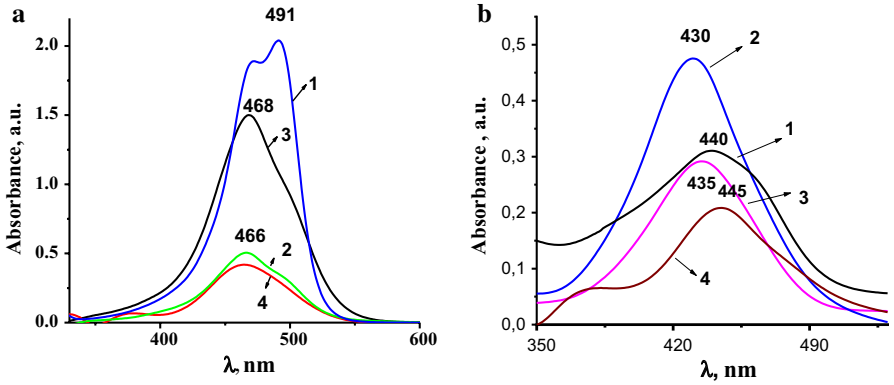

Fig. 3 Absorption spectra **a** of AO and **b** of AY: 5×10^{-5} M aqueous solution (1), adsorbed on SiO_2 (2), TiO_2/SiO_2 (3) and TiO_2 (4)

by a shift of the absorption band maximum to a short-wavelength region from 490 nm in a solution to 470 nm for AO adsorbed on TiO_2 and SiO_2 films. A broad band for AY absorption masked the spectrum of its dimeric form. The absorption maximum at 442 nm corresponded to the monomeric form in solution. However, it was shown in [31] that the increase of the AY amount on SiO_2 caused a bathochromic shift of the fluorescence maximum with the emission intensity decrease. This is explained by formation of associates of various structures. Blue-shift of the absorption maximum from 440 to 435 nm and 430 nm indicates a similar situation for AY on SiO_2/TiO_2 and SiO_2 film with stronger acidic sites, resulting in both protonation and dimerization processes.

On titania film, the adsorption of this dye (AY) is accompanied by a red-shift in the position of the maximum from 440 to 445 nm, which is an indicator of the formation of dimeric associates of different spatial structures. It is known that protonation of acridine dyes proceeds via proton coordination to a nitrogen atom of an aromatic ring causing a bathochromic shift of the absorption spectrum [32]. Further protonation of acridine dyes through basic N-dimethylamino groups by acidic OH groups of mixed oxide surface [33, 34] with formation of double ions is accompanied by a shift of the absorption band towards shorter wavelengths [22, 35]. These data are in good agreement with the theoretical calculations performed in [23].

The desorption/ionization spectra of the dyes desorbed from the surface of mesoporous oxide films (Fig. 4) record a number of peaks that are absent in the mass spectra of LDIs from the steel substrate. The monomolecular adsorption is accompanied by desorption of cationic forms of acridine dyes $[M+H]^+$. Adsorption of dyes in the form of dimers and associates results in the presence of a two-charge ion dimer $[2M+3]^{2+}$ in the mass spectra of LDI as well as the products of thermoionization and oxidation–reduction processes, $M^{+\cdot}$, $[M-H]^+$ and $[M+2H]^+$, formed by laser irradiation of UV range.

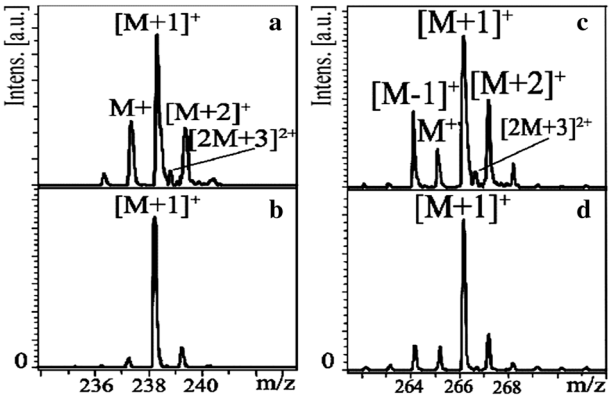

Fig. 4 Intensity distribution of some peaks in LDI mass spectra of AY (**a**, **b**) and AO (**c**, **d**) dyes adsorbed on mesoporous TiO_2 films

Effect of film composition on the process of adsorbed dye photodegradation

The fixation of the intermediates of adsorbed cationic dye photodegradation products allows us to recognize the differences in the mechanisms of photoreactions on the surface and efficiency of photocatalytic processes. The reduced form of MB is considered [16] as an intermediate of the UV-stimulated catalytic decomposition, the initial stage of which is demethylation. The dynamics of changes in the mass spectra of MB adsorbed on TiO_2 film during irradiation for 45 min indicates that the intensity of the peak of a semi-reduced form of MB is decreased with time, while the intensity of demethylated fragments is increased step by step reflecting the degree of photodestruction of the dye (Fig. 5). The most efficient process occurs on titania and titanium-silica substrates which is confirmed by the data of absorption spectra. Depending on the type of substrate and the duration of irradiation, the changes in the ratio of the intensities of the semi-reduced form of MB to the original cation peaks are also observed. The most pronounced

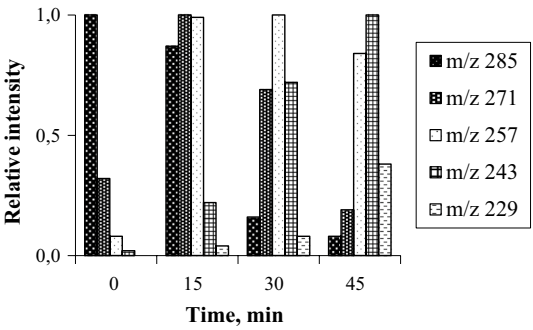

Fig. 5 Dependence of the relative intensity of the peaks of demethylated fragments of MB adsorbed on TiO_2 film on the UV irradiation duration

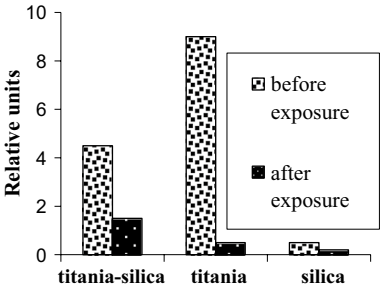

Fig. 6 Intensity ratio of $[M+H]^{+}$ to M + ion peaks in the mass spectra of adsorbed MB before and after 45 min of UV irradiation

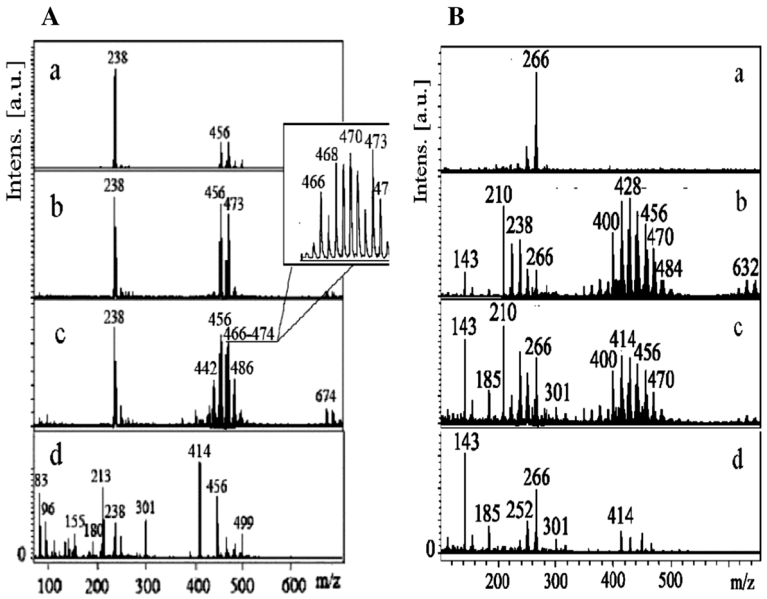

Fig. 7 Changes in the mass spectra of AY (**A**) and AO (**B**) adsorbed on TiO_2 films: before irradiation (a), after 15 min (b), 30 min (c) and 45 min (d) of irradiation

difference between the values of this ratio between irradiated and non-irradiated adsorbates is observed for TiO_2 films (Fig. 6).

As a result of UV irradiation of acridine dyes adsorbed on the catalytically active films, the effect of significant enrichment of mass spectra by products of photodimerization and their fragments can be revealed (Fig. 7). The LDI mass spectra of AY show that the irradiation of this dye adsorbed on TiO_2 leads to the formation of dimeric associates of various compositions that are the species of degradation during subsequent photoreactions.

In the case of AO, the peaks of the original cation fragments are observed simultaneously with peaks corresponding to dimeric associates of different masses in the mass spectra of irradiated samples. We can conclude that the reactions of dye cation's demethylated fragments' association with contribution to the intensity of m/z

peaks at 400, 414, 428, 442, 456, 470 and 484 should be also assumed in addition to the destruction processes of the dimer structures (considered for AY). The well-known metachromatic effect, i.e. a change of dye color upon adsorption on a hydrophilic surface due to aggregation process, occurred in addition to a hypsochromic shift of the absorption band [24, 29, 36].

These spectral changes coincided in time (10–15 min after the start of irradiation) with the appearance of the photogenerated superhydrophilicity of the TiO_2 surface. Within the first minutes of irradiation, the contact wetting angle fell from 32° for non-irradiated film to ~ 0° for irradiated sample [24]. These phenomena can raise the sensitivity of the method and eliminate the use of mesoporous films with controlled hydrophilicity as substrates in the LDI experiment. The hypsochromic shift in the AO spectrum was a sign of the formation of so-called H aggregates (molecules packed into a sandwich structure). The bathochromic shift in AY spectra was characteristic of the formation of J aggregates (molecules packed like bricks) [37].

The signals of the aggregates weakened with irradiation time for both dyes. The products with m/z = 180, 156, 143, 132, 122, 108, 96 and 83 and less appeared as a result of extensive oxidative degradation of the dye [20, 21] that was photocatalytic in nature and was accompanied by the destruction of the aromatic ring. The photodegradation mechanism of acridine dyes in the presence of TiO_2 included injection of an electron into the semiconductor conduction band [16] with subsequent oxidation of the resulting cation radicals by active oxygen radicals. This was evident in the appearance of the products with masses less than the mass of acridine that was accompanied by the destruction of the aromatic ring and cleavage of the benzene ring.

The absence of the peaks of dimeric associates in the LDI mass spectra of AO on the SiO_2 film surface for both non-irradiated and irradiated samples and the simultaneous presence of the peak of a two-charge dimer ion are obviously an indicator of the absence of an active effect of the SiO_2 on the energy transformation in excited dye molecules.

Thus, among the investigated substrates, the most conducive to the formation of dimeric associates are TiO_2 films, and this effect correlates with the degree of their photocatalytic activity.

Effect of doping silica films with silver nanoparticles on the efficiency of ion formation of adsorbed molecules

Acting as an accumulator/transmitter of UV laser light, silver nanoparticles (Ag NPs) with the size of 10–160 nm were found to assist in desorption/ionization of biomolecules with little or no induced fragmentation [38–41]. They were used for identification of amyloid beta oligomers [38], estrogens [39], peptides [40], cysteine and homocysteine in human urine [41] by LDI-MS. In respect to mass spectrometry, the Ag NPs with the size smaller than 10 nm have not been investigated in detail. Previous mass spectrometric study of NPs, namely Ag and Au, have revealed that the ion yield efficiency is dependent on the wavelength of the exciting laser as well as on the NPs' size, shape, agglomeration [42] and the quantity of NPs per nm^2 of

surface [43]. At laser wavelengths different from that which correspond to local surface plasmon resonance (LSPR), especially at wavelengths longer then the peak of plasmon absorption, the ability to generate a detectable ion signal decreased rapidly [43]. The influence of silver NPs incorporated in the silicon substrate on the amplification of the mass spectrometric signal of the analyte has been investigated. The growth of the ion yield is discussed on the basis of the phenomena of photo-induced local heating of the surface of the ionization substrate and the localized plasmon resonance (LPR) of the silver NPs arising from the absorption of laser radiation.

According to our previous study [42], the silica film structure is slightly ordered, keeping certain areas of the hexagonal mesostructure with the mean pore size of ~ 10 nm and $S_{BET} = 650\ m^2/g$. The conditions of heat processing allow control of the following film characteristics: the purity, stability, porosity and size of Ag NPs. The temperature range and duration of annealing have been selected to ensure the removal of pore-forming organic material, the creation of mesoporous SiO_2 framework, and the thermoreduction of Ag. The pore structure of films influences the formation of Ag NPs with a uniform size distribution. At the heating stage, Ag clusters and particles change their morphology and location in the film (in pores or at the outer surface of the film depending on the size of particles and pores, mass transfer processes, etc.). Composites with Ag NPs/porous oxide films demonstrate certain changes in the pore structure in comparison with those of individual oxide films. In the case of silica, silver doping leads to the formation of secondary porosity with much larger pores. SEM images show a relatively uniform distribution of AG NPs deposited predominantly at the outer surface and entrapped into subsurface layer in the thin silica films.

According to the described method, the different duration and temperature of annealing of mesoporous silica samples cause the changes in the size of spherical NPs in the range of 2–12 nm and a relative shift of the optical absorption maximum [44], changes in the resonance peak intensity and in the UV spectrum curve view.

The absorption spectrum (Fig. 8) of the film treated at 400 °C (dashed curve) shows a maximum near 380 nm that originates from Ag nanoparticles on SiO_2 surface [45] and a wide band with a diffuse maximum around 423 nm. The authors [46, 47] attribute the latter to the weak LSPR of small-sized (under 4 nm) Ag NPs. As compared with the LSPR maximum of Ag NPs of 5–12 nm size (solid curve), it is effectively red-shifted. Its height decreases dramatically while the spectral width become broader. These effects are related to a wide distribution of particle sizes in the host matrix as well as to a quantum size effect for NPs $\leq$ 4 nm [47–49].

The increase in the bulk concentration of $AgNO_3$ in the film precursor from 3 to 10% has no influence on the peak position in the electronic spectra of resulting nanocomposites. It means that under the given synthesis technique, the Ag NPs size is insignificantly changed at the Ag concentration within the mentioned range whereas the number of NPs per surface area unit depends on the concentration.

The increase of the calculation temperature up to 450 °C results in the coalescence of Ag NPs. Their growth leads to the changes in the UV-spectra. For the samples treated at 450 °C, the absorption spectrum (Fig. 8a solid curve) exhibits an intense broad band at 400 nm which is the characteristic local surface plasmon resonance band (owing to the coherent oscillation of electrons in the conduction band of Ag

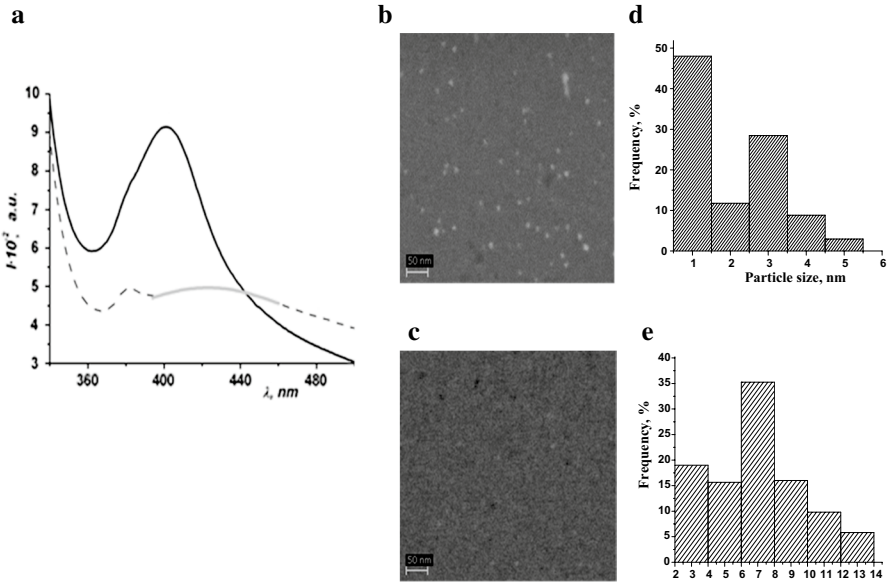

Fig. 8 Absorption spectra of Ag/SiO_2 films treated at 400 °C (**a**, dash curve) and 450 °C (**a**, solid curve); SEM images and corresponding size distribution histograms of Ag/SiO_2 films treated at 400 °C (**b**, **d**) and at 450 °C (**c**, **e**)

NPs). SEM images reveal that the obtained films contain spherical Ag NPs with the diameter of 5 ÷ 12 nm (Fig. 8c) and the surface density of $(2 \div 2.4) \times 10^3$ NPs μm^{-2}. Figure 8b, c shows the SEM images of Ag/SiO_2 films treated at 400 and 450 °C with the corresponding histograms demonstrating the size distribution of Ag nanoparticles. The AG NPs have the spherical shape with different diameters of the particles estimated for different samples: $d \leq 4$ nm for Ag/SiO_2 (400 °C) and $d \approx 5$–12 nm for Ag/SiO_2 (450 °C). Thus, the heat treatment of nanocomposites with Ag content within 3–10% at 400 °C leads to the formation of Ag NPs smaller than 4 nm. The higher calcination temperature (450 °C) leads to the agglomeration of Ag NPs (Fig. 8d vs. e). The SEM results indicate a large separation between NPs, so that the electrodynamic coupling does not affect their optical spectra.

The positive ion mass-spectra of MB adsorbed on the surface of silica films doped with Ag NPs of different concentrations were compared. To get qualitative mass spectra of the dye, these samples required lower laser power than MB samples adsorbed on pure SiO_2. In the mass spectra of all investigated substrates, the main peaks were in the area of the dye cation M^+ with the molecular weight of 284 Da. It has been demonstrated that there is a correlation between the ion yield of MB cations adsorbed on the surface of the silica matrix containing Ag NPs and the dimensions of NPs. The measurements showed a variation of the MB cation peak intensity on the silver concentration in nanocomposite. It is clearly seen that an increase in the Ag ion concentration from 3 to 10% in the films treated at 400 °C causes the fivefold increase of the MB cation desorption peak intensity (Fig. 9a). It indicates a stimulating effect of Ag NPs in the silica matrix on the

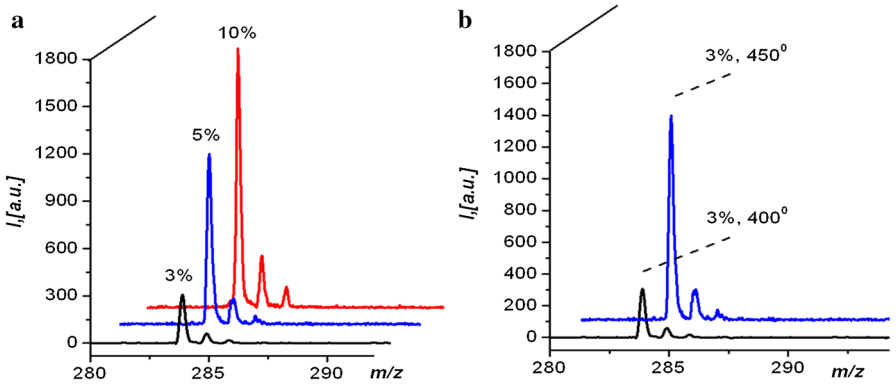

Fig. 9 Intensity dependence of positive ion LDI peaks of MB adsorbed onto Ag/SiO_2 films calcined at 400 °C on different content of $AgNO_3$ in silica sol (**a**) and on the treatment temperature for the samples with 3% of $AgNO_3$ (**b**)

process of the desorption/ionization of adsorbed MB cations. It is supposed that a more effective transfer of the laser energy to adsorbed MB cations takes place in this case, and the photoinduced heating of the composite surface is the main factor having an impact upon desorption/ionization efficiency. Considering the ratio of the absorption coefficient of UV laser irradiation and the heat conductivity of metal NPs and the silica matrix, we can conclude that NPs are the more active component in the process of the energy transfer. A portion of NPs' thermal energy (its excess originates from the optical excitation) passes to the bulk of the porous matrix, locally elevating the surrounding temperature and, perhaps, weakening the interaction of MB with the substrate. The degree of NP aggregation also affects the heat transmission significantly. The temperature increase appeared in the system can be strongly enhanced due to an accumulative effect and Coulomb interaction [50].

As an important parameter influencing ion formation, the total NP surface area has been denoted [42]. Taking into account these considerations, an intensification of the ion yield of the test compound (Fig. 9a) is expected at higher concentration of Ag NPs in the silica matrix. At homogeneous Ag NP distribution on the substrate surface, an additional effect of the Ag concentration growth up to 10% is observed in the gradual increase of ion yield.

The key distinction in the electronic spectra of nanocomposites (Fig. 8a) annealed at different temperatures appears in the presence of an enhancement in the absorption of photons with wavelengths characteristic of the LSPR. This phenomenon is observed for the substrates treated at 450 °C. The MB cation peak intensity has been found to be near three times higher in comparison with the composites treated at 400 °C with the same Ag content (Fig. 9b). So, there is an explicit connection between the ion signal intensity and the effect of LSPR. As a result of heat treatment at $T > 400$ °C, the conglomeration of Ag NPs into bigger (5–12 nm) ones is achieved. Absorbing more UV radiation quanta, such particles strongly stimulate the process of MB desorption and ion formation.

Clarifying the ionic current increase in the case of 5–12-nm Ag NPs, apart from the factors of local heating and the drastic specific particle surface growth, we should consider several other parameters. It is known that the interaction of the pulsed UV light with a silver nanoparticle of the average size of 8 nm leads to a strong photoluminescence (PL) from silver because of radiative electron interband transitions and the radiative decay of the surface plasmons in AG NPs [51]. The experimental data point out the dependence of the intensity and peak position in PL spectra of Ag/SiO_2 composites on the excitation wavelength and sizes of AG NPs. It has been revealed that the shift of the bands in the PL spectra can be caused by the strong coupling of the emitted photon to the LSPR band. Authors of the "surface plasmon-photon" polariton coupling hypothesis [51] supposed that as a result of such coupling, the states of the emitted photon and surface plasmon can attract each other, resulting in the shift of the photon energy value to the LSPR side.

An effective mechanism of energy transfer in the discussed "dye-metallic nanoparticle" system can involve local surface plasmons. Resonant processes cause the maximum enhancement of local electric fields close to the surface of the particles and improve the effectiveness of the transfer of the plasmon excitation energy to dye molecules. It has been found that the contribution of the plasmon mechanism to the total rate of energy transfer dominates (exceeds the rate of transfer by one to two orders of magnitude in the absence of conducting species in the system) when the molecules are close to the metal surface [52]. Photo-desorption is directly dependent on the quenching rate of electronic excitation. It rises substantially at the resonance of optical radiation with plasmon oscillations of metallic NPs due to a light wave field gain on their surface.

The role of local heating is also considered for the samples annealed at 450 °C. The resultant evolved heat depends not only on the number of NPs but on the inter-NP distance and NP arrangement. Clustering of metal NPs can significantly affect the total heat generation. Moreover, as follows from previous experiments [50], the heat generation becomes especially strong in the case of metal NPs in the regime of plasmon resonance.

LDI experiments applying the laser wavelength at 337 nm reveal an effective stimulation of the MB ion generation on the surface of Ag/SiO_2 composites and the existence of some interesting relationships between substrate features and mass spectra intensities. Thus, the presence of Ag NPs at the surface of the tested substrates promotes efficient energy transfer to adsorbed molecules as shown by LDI investigation. The interaction of laser radiation with Ag NPs leads to several processes, such as local heating, LSPR and PL. However, we assume that the local heating and LSPR are dominating processes for the substrates containing Ag NPs with the size lower than 4 nm and for 5-12 nm, respectively.

Conclusions

- Photodegradation of adsorbed dyes on the surface of porous transparent TiO_2, TiO_2/SiO_2 and SiO_2 films leads to the formation of various transient intermediates depending on the film composition. In the presence of titania, photobleach-

ing of adsorbed MB, AO and AY occurred faster compare to pure silica. We suggest that formation of active oxidative species like singlet oxygen and/or hydroxyl radical under UV irradiation leads to the complete degradation and discoloration of adsorbed dye. Photodegradation efficiency of adsorbed MB, AO and AY were observed in the order of $TiO_2 > TiO_2/SiO_2 > SiO_2$.

- Metachromasy effects (the dye aggregation followed by change of color with a hypsochromic spectral shift due to repulsive interactions, which induce shifts to higher energies) coincide with photoinduced superhydrophylicity of TiO_2 films.
- The combination of electronic spectroscopy and LDI-MS methods facilitates obtaining reliable data on the mechanisms and kinetics of dye molecule destruction taking place under UV irradiation in situ on the surface of photocatalytically active mesoporous films. Efficient photodegradation of thiasine and acridine dyes occurs through the following steps: N-demethylation (deamination for AY); photodimerization; photodegradation.
- The use of mesoporous oxide films appears to be prospective for the development of methodical approaches for investigation of lower molar mass molecules by LDI. The films as the LDI substrates seem to be attractive due to the controllable film porosity and morphology modification. The combination of an inert film and Ag NPs has significant advantages over other matrix-free approaches, providing the possibility to control the size and aggregation degree of metal NPs.

References

1. U. Bach, D. Lupo, P. Comte, J.E. Moser, F. Weissörtel, J. Salbeck, H. Spreitzer, M. Gratzel, Nature **395**, 583 (1998)
2. A.M. Amata, A. Arquesa, F. Galindob, M.A. Mirandac, L. Santos-Juanesa, R.F. Verchera, R. Vicentea, Appl. Catal. B **73**, 220 (1997)
3. V.P.S. Pereira, P.K.D.D.P. Pitigala, P.V.V. Jayaweera, K.M.P. Bandaranayake, K. Tennakone, J. Phys. Chem. B **107**, 13758 (2010)
4. R. Mosurkal, L. Hoke, S.A. Fossey, L.A. Samuelson, J. Kumar, D. Waller, J. Macromol. Sci. Pure Appl. Chem. **43**, 1907 (2006)
5. A.K. Jana, J. Photochem. Photobiol. A Chem. **132**, 1 (2000)
6. A.K. Jana, B.B. Bhowmik, J. Photochem. Photobiol. A Chem. **122**, 53 (1999)
7. T. Wu, G. Liu, J. Zhao, H. Hidaka, N. Serpone, J. Phys. Chem. **102**, 5845 (1998)
8. Yu. Gnatyuk, N. Smirnova, A. Eremenko, V. Ilyin, J. Adsorpt. Sci. Technol. **23**, 497 (2005)
9. G.V. Krylova, YuI Gnatyuk, N.P. Smirnova, A.M. Eremenko, V.M. Gunko, J. Sol–Gel. Sci. Technol. **50**, 216 (2009)
10. G.V. Krylova, A.M. Eremenko, N.P. Smirnova, S. Yustis, Theor. Éxp. Chem. **41**, 100 (2005)
11. D.A. Makarov, N.A. Kuznetsova, O.L. Kaliya, Zhurnal Fizicheskoi Khimii **80**, 336 (2006)
12. G. Starukh, S. Toscani, S. Boursicot, L. Spanhel, Z. für Phys. Chem. **221**, 349 (2007)
13. F.B. Li, X.Z. Li, Appl. Catal. A **228**, 15 (2002)
14. S. Horikoshi, H. Hidaka, N. Serpone, J. Photochem. Photobiol. A Chem. **153**, 185 (2002)
15. Ying Ma, Jian-ian Yao, J. Photochem. Photobiol. **116**, 167 (1998)
16. A. Mills, J.S. Wang, J. Photochem. Photobiol. A: Chem. **127**, 123 (1999)
17. H. Gnaser, M.R. Savina, W.F. Calaway, C.E. Tripa, I.V. Veryovkin, M.J. Pellin, Int. J. Mass Spectrom. **245**, 61 (2005)
18. H. Gnaser, A. Orendorz, C. Ziegler, E. Rowlett, W. Bock, Appl. Surf. Sci. **252**, 6996 (2006)
19. O. Linnik, E. Manuilov, S. Snegir, N. Smirnova, A. Eremenko, J. Adv. Oxid. Technol. **12**, 265 (2009)

20. T.A. Fesenko, N.I. Surovtseva, V.A. Pokrovsky, A.M. Eremenko, N.P. Smirnova, Mass Spectrom. **4**, 289 (2007). **(in Russian)**
21. N.I. Surovtseva, A.M. Eremenko, N.P. Smirnova, V.A. Pokrovsky, T.A. Fesenko, G.N. Starukh, Theor. Exp. Chem. **43**, 220 (2007)
22. N.I. Surovtseva, N.P. Smirnova, T.V. Fesenko, YuI Gnatyuk, A.M. Eremenko, V.A. Pokrovskiy, J. Adv. Oxid Technol. **11**, 551 (2008)
23. N.P. Smirnova, N.I. Surovtseva, T.V. Fesenko, E.M. Demianenko, A.G. Grebenyuk, A.M. Eremenko, J. Nanostruct. Chem. **5**, 333 (2015)
24. N. Smirnova, T. Fesenko, M. Zhukovsky, J. Goworek, A. Eremenko, Nanoscale Res. Lett. **10**, 500 (2015)
25. T.V. Fesenko, S.V. Snegir, N.I. Surovtseva, N.P. Smirnova, V.A. Pokrovsky, Chem. Phys. Technol. Surf. **4**, 276 (2013)
26. A.C. Pratt, Photochemistry **30**, 230 (1999)
27. S.N. Guha, J.P. Mittal, J. Photochem. Photobiol. A Chem. **92**, 181 (1995)
28. T. Zhang, T. Oyama, A. Aoshima, H. Hidaka, J. Zhao, N. Serpone, J. Photochem. Photobiol. A Chem. **140**, 163 (2001)
29. E. Stathatos, P. Lianos, C. Tsakiroglou, Langmuir **20**, 9103 (2004)
30. S. Coon, T. Zakharian, N. Littlefield, V. Pak, Langmuir **16**, 9690 (2000)
31. V.K. Runov, Zhurnal Fizicheskoi Khimii **72**, 933 (1998)
32. N.N. Vlasova, L.P. Golovkova, N.G. Stukalina, Colloid J. **74**, 25 (2012)
33. D.R. Worrall, S. Williams, A. Eremenko, N. Smirnova, O. Yakimenko, G. Staruch, Colloids Surf. A: Physicochem. Eng. Asp. **230**, 45 (2004)
34. S. Imamura, S. Ishida, H. Tarumoto, Y. Saito, T. Ito, J. Chem. Soc. Faraday Trans. **89**, 757 (1993)
35. A.M. Eremenko, N.P. Smirnova, V.M. Ogenko, A.A. Chuiko, Res. Chem. Intermed. **19**, 855 (1993)
36. T.H. James, *The Theory of the Photographic Process*, 4th edn. (Macmillan, New York, 1977)
37. E. Gallopini, S. Thyagarajan, The Spectrum **18**, 25 (2005)
38. T. Yonezawa, H. Kawasaki, A. Tarui et al., Anal. Sci. **25**, 339 (2009)
39. T.-C. Chiu, L.-C. Chang, C.-K. Chiang, H.-T. Chang, J. Am. Soc. Mass Spectrom. **19**, 1343 (2008)
40. L. Hua, J. Chen, L. Ge, S.N. Tan, J. Nanopart. Res. **9**, 1133 (2007)
41. K. Shrivas, H.-F. Wu, Rapid Commun. Mass Spectrom. **22**, 2863 (2008)
42. M.T. Spencer, H. Furutani, S.J. Oldenburg et al., J. Phys. Chem. C **112**, 4083 (2008)
43. K. Awazu, M. Fujimaki, C. Rockstuhl et al., J. Am. Chem. Soc. **130**, 1676 (2008)
44. W. Cai, H. Hofmeister, T. Rainer, Phys. E **11**, 339 (2001)
45. L. Yang, G.H. Li, J.G. Zhang, L.D. Zhang, Appl. Phys. Lett. **78**, 102 (2001)
46. H. Bi, W. Cai, H. Shi, X. Liu, Chem. Phys. Lett. **57**, 249 (2002)
47. S. Peng, J.M. McMahon, G.C. Schatz, S.K. Gray, Y. Sun, PNAS **107**, 14530 (2010)
48. M.A. Smithard, Solid State Commun. **13**, 153 (1973)
49. K.P. Charlé, F. Frank, W. Schulze, Ber. Bunsenges. Phys. Chem. **88**, 350 (1984)
50. A.O. Govorov, H.H. Richardson, Nano Today **2**, 30 (2007)
51. O.A. Yeshchenko, I.M. Dmitruk, A.A. Alexeenko et al., Phys. Rev. B **79**, 235438 (2009)
52. M.G. Kucherenko, T.M. Chmereva, D.A. Kislov, High Energy Chem. **43**, 587 (2009)

Affiliations

N. Smirnova[1] · A. Eremenko[1] · T. Fesenko[1] · M. Kosevich[2] · S. Snegir[1]

[1] Chuiko Institute of Surface Chemistry of NASU, 17 General Naumov str., Kyiv 03164, Ukraine

[2] Verkin Institute for Low Temperature Physics and Engineering of NASU, 47 Ave. Science, Kharkiv 61103, Ukraine